Journal of Photochemistry & Photobiology, A: Chemistry 452 (2024) 115544

Contents lists available at ScienceDirect

Journal of Photochemistry & Photobiology, A: Chemistry

journal homepage: www.elsevier.com/locate/jphotochem

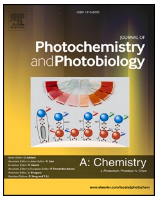

Amino-functionalized iron-based MOFs for Rhodamine B degradation in heterogeneous photo-Fenton system

Lei-Qin Sun [a], Xiao-Fang Shen [a,b], Hong-Ming Zhang [a], Yue-Hong Pang [a,b,*]

[a] State Key Laboratory of Food Science and Resources, School of Food Science and Technology, Collaborative Innovation Center of Food Safety and Quality Control in Jiangsu Province, Jiangnan University, Wuxi 214122, China

[b] International Joint Laboratory on Food Safety, Jiangnan University, Wuxi 214122, China

ARTICLE INFO

Keywords:
Rhodamine B
Iron-based MOFs
Amino-functionalization
Wastewater treatment
Heterogeneous photo-Fenton

ABSTRACT

Amino-functionalized iron-based MOFs were successfully synthesized and used for the photo-Fenton-catalyzed degradation of Rhodamine B (RhB). The degradation efficiency of NH_2-MIL-53(Fe) towards RhB (95.0%) exceeded that of NH_2-MIL-88B(Fe) (87.0%) and NH_2-MIL-101(Fe) (88.0%), which might be mainly because that NH_2-MIL-53(Fe) had the most suitable specific surface area and pore volume, and the best light absorption properties. Additionally, NH_2-MIL-53(Fe) exhibited higher degradation efficiency than MIL-53(Fe) (84.0%), possibly owing to the incorporation of amino functional groups that inhibited the recombination of photo-generated electron-hole pairs and enhanced visible light responsiveness. Remarkably, NH_2-MIL-53(Fe) had a good degradation effect on RhB in a wide range of pH (3.0–7.0), and the degradation rate was still as high as 90.0% after 5 consecutive degradation experiments. The degradation process was predominantly influenced by the involvement of $\cdot$OH and $^1O_2$, as evidenced by the outcomes of free radical capture experiments. Possible degradation pathways of RhB were proposed by mass spectrometry.

1. Introduction

Water pollution is a worldwide problem, which has become more and more serious in the last decades and posed a threat to the ecosystem due to population growth as well as human activities [1]. The printing and dyeing, medical, and agricultural industries generate large amounts of organic wastewater. Most of the organic pollutants in these wastewaters, such as dyes, antibiotics, and pesticides, are toxic and difficult to degrade [2–4]. Rhodamine B (RhB) is a prevalent biological dye [5], which is extensively used in textile, leather, printing and dyeing, and paper-making industries [6]. RhB poses a carcinogenic and mutagenic risk to living species [7]. Therefore, the complete removal of RhB from industrial wastewater is of utmost importance.

The most common methods for treating organic pollutants from wastewater include adsorption, biodegradation, and chemical reduction and oxidation [8,9]. Among them, adsorption is the most widely employed technology for removing organic pollutants from wastewater [10,11]. It can effectively remove pollutants, but it cannot degrade them [12–14]. Biodegradation method employs the metabolic capacity of microorganisms to transform organic compounds in wastewater into inorganic compounds, which is low efficiency and high cost [15]. Traditional chemical reduction and oxidation technology to degrade organic pollutants also has some limitations, such as the generation of a large amount of sludge in treatment [15–17], so how to develop a green, sustainable and efficient wastewater treatment method is still an important problem.

Advanced oxidation processes (AOPs) are an efficient way to treat difficult-to-degrade organics, including photocatalysis, microwave catalysis and photo-Fenton process etc. [18–20]. Among them, the photo-Fenton process has shown significant advantages in wastewater treatment owing to simple operational procedures and low energy requirements. The traditional photo-Fenton process has limited applicability due to its extremely narrow pH operating range (2.0–3.5), the formation of substantial quantities of iron sludge, and low utilization of H_2O_2 [16,21]. Additionally, the unrecoverable iron ions may cause secondary pollution. The heterogeneous photo-Fenton process utilizes solid catalysts instead of soluble Fe(II) or Fe(III), with a wide reaction pH range and recyclable catalysts [22,23]. At present, the development of heterogeneous photocatalysts with green efficiency and excellent catalytic activity is still very important.

---

[*] Corresponding author at: State Key Laboratory of Food Science and Resources, School of Food Science and Technology, Collaborative Innovation Center of Food Safety and Quality Control in Jiangsu Province, Jiangnan University, Wuxi 214122, China.

E-mail address: yhpang@jiangnan.edu.cn (Y.-H. Pang).

https://doi.org/10.1016/j.jphotochem.2024.115544
Received 4 January 2024; Received in revised form 13 February 2024; Accepted 19 February 2024

Metal-organic frameworks (MOFs) are a promising class of porous materials composed of metal ion clusters linked by organic linkers via strong covalent bonds to form extended networks [24,25]. Due to their high surface area, high porosity, potentially high density of active sites, controllable morphology and certain stability [19,26], MOFs have garnered significant attention in the field of adsorption and heterogeneous catalysis [27–30]. Among the various types of MOFs, iron metal–organic frameworks (Fe-MOFs) have garnered growing interest due to their environmental friendliness, chemical adjustability and cost effectiveness. Notably, several Fe-MOFs have been demonstrated to exhibit significant absorption capabilities within the visible region, thanks to the abundance of iron-oxygen (Fe-O) clusters present [31,32]. These clusters tend to produce holes and photogenerated electrons. Photogenerated electrons possess a pronounced ability for reduction and can in-situ reduce Fe(III) to Fe(II) on the surface of Fe-MOFs. Upon the addition of H_2O_2, Fe(II) reacts with it to generate a substantial quantity of ·OH, which can be capable of degrading organic pollutants. The utilization of Fe-MOFs as catalysts has been widely reported for photocatalytic degradation [33] and oxygen evolution [34]. Therefore, Fe-MOFs can be applied to Fenton systems driven by visible light. Functional groups can be introduced into the organic linkers of Fe-MOFs to tune the separation and migration of photogenerated electron-hole [35]. The introduction of -Br and $–NO_2$ into terephthalic acid favors the Fenton activity of MIL-88B(Fe) [36]. Amino-functionalized iron-based MOFs have good catalytic performance and the ability to regulate photogenerated electron-hole separation and migration. To our knowledge, there have been few systematic investigations by researchers into the photo-Fenton performance (PFP) of amino-functionalized Fe-MOFs as visible light-driven Fenton-like catalysts.

Herein, amino-functionalized Fe-MOFs (NH_2-MIL-53, NH_2-MIL-88B and NH_2-MIL-101) were successfully synthesized and used for the degradation of RhB. The surface properties and microstructures of catalysts were characterized, and the effects of pH, catalyst dosage, H_2O_2 concentration, and inorganic anions on the catalytic degradation performance were systematically investigated. Reactive oxygen species (ROS) of the reaction were explored by free radical capture experiments. The intermediates of RhB were determined by mass spectrometry (MS), and the degradation pathways of RhB were proposed. NH_2-MIL-53(Fe) is expected to be used in heterogeneous photo-Fenton treatment of complex actual wastewater.

2. Materials and methods

2.1. Chemicals and reagents

Chemicals and reagents were described in **Text S1**.

2.2. Synthesis of Fe-MOFs

The synthesis of NH_2-MIL-53(Fe) was conducted following the procedures described in the previously published literature [37]. A solution was prepared by dissolving equimolar amounts of $FeCl_3·6H_2O$ and 2-Aminoterephthalic acid (H_2ATA) in 36 mL DMF, followed by stirring for 30 min. The mixed solution underwent hydrothermal treatment at 150℃ for 24 h. Following the cooling process, the products was washed three times with DMF and methanol. The ultimate product was subjected to drying at 60℃. The synthesis of MIL-53(Fe) was used a comparable approach.

The synthesis of NH_2-MIL-88B(Fe) and NH_2-MIL-101(Fe) was described in **Text S2**.

2.3. Characterization

The detailed information about the characterization was shown in **Text S3**.

2.4. Heterogeneous photo-Fenton degradation of RhB in aqueous solution

The specific degrading procedures were described in **Text S4**.

3. Results and discussion

3.1. Characterization

SEM images of MIL-53(Fe) and NH_2-MIL-53(Fe) were shown in Fig. 1**a** and Fig. 1**b**. It could be shown that MIL-53(Fe) had a spindle octahedral structure. Meanwhile, the images of NH_2-MIL-53(Fe) closely resembles that of MIL-53(Fe), indicating that the introduction of $–NH_2$ did not affect the lattice structure of NH_2-MIL-53(Fe).

The FT-IR spectra were shown in Fig. 1**c**. The wavelength at approximately 572 cm^{-1} might be the Fe-O band stretching vibration caused by the interaction of Fe(III) with terephthalic acid or H_2-ATA, indicating the presence of Fe-O clusters [38]. The peaks at approximately 3460 and 3340 cm^{-1} were attributed to the symmetrical and asymmetrical stretching vibration of $–NH_2$, respectively [39]. This provided strong support for enhancing the adsorption capacity of NH_2-MIL-53(Fe). The FT-IR spectra of NH_2-MIL-88B(Fe) and NH_2-MIL-101 (Fe) exhibited similarities to NH_2-MIL-53(Fe), in agreement with the findings reported in the literature [40,41].

The XRD patterns were employed for the purpose of determining the crystal phase of the materials that were prepared. As shown in Fig. 1**d**, the characteristic peaks of the prepared four materials were in accordance with those reported literature [38,41–45]. In addition, compared with NH_2-MIL-88B(Fe), NH_2-MIL-101(Fe) and MIL-53(Fe), NH_2-MIL-53 (Fe) exhibited intense and sharp peaks in its XRD spectrum, indicating a high degree of crystallinity [46–48].

The Fe 2p spectra of MIL-53(Fe) and NH_2-MIL-53(Fe) were shown in Fig. S1**b** and Fig. 2**b**. The characteristic peaks observed at 711.8 and 724.6 eV correspond to the Fe $2p_{3/2}$ and Fe $2p_{1/2}$, respectively. These two peaks usually indicated the presence of Fe(III) [42]. In Fig. S1**c**, the peaks of C 1 s in MIL-53(Fe) centered at 284.8, 286.6 and 288.7 eV, matching with C = C, C-O and C = O [49]. Amusingly, the characteristic peaks of C 1 s in NH_2-MIL-53(Fe) were observed at 284.8, 286.3 and 288.6 eV (Fig. 2**c**). In contrast to the peak at 286.6 eV, a peak centered at 286.3 eV could be caused by the presence of C-N [50]. The spectra of N 1 s in NH_2-MIL-53(Fe) contained two peaks at 399.2 and 400.6 eV (Fig. 2**d**), corresponding to C-N or N-H [51,52].

3.2. Photo-Fenton degradation performance

In order to evaluate the PFP of synthesized amino-functionalized Fe-MOFs, RhB degradation experiments were carried out under H_2O_2 and visible light. As shown in Fig. 3**a**, all amino-functionalized Fe-MOFs showed good degradation effects on RhB, suggesting their potential as catalysts for visible-light-driven Fenton-like reactions. The degradation efficiency of NH_2-MIL-53(Fe) towards RhB (95.0%) exceeded that of NH_2-MIL-88B(Fe) (87.0%) and NH_2-MIL-101(Fe) (88.0%). The degradation process of pollutants was further analyzed using the pseudo-zero-order and pseudo-second-order kinetics model (**Table S1**) and pseudo-first-order kinetics model (Fig. 3**b)**.

By comparing the correlation coefficient (R^2) value from the three models (zero order, first order, and second order), it was evident that the first-order kinetic model outperformed both the zero-order and second-order kinetic models in representing the photo-Fenton degradation of RhB. The degradation rate constants of NH_2-MIL-53(Fe) (0.0225 min^{-1}) were higher than those of NH_2-MIL-88B(Fe) (0.0123 min^{-1}) and NH_2-MIL-101 (0.0176 min^{-1}). Thus, NH_2-MIL-53(Fe) exhibited the most superior photo-Fenton activity when subjected to visible light irradiation. In comparison to other recently reported catalysts (**Table S2**), NH_2-MIL-53(Fe) also exhibited notable advantages in the degradation of RhB, thereby underscoring its substantial potential as a photo-Fenton catalyst in practical applications.

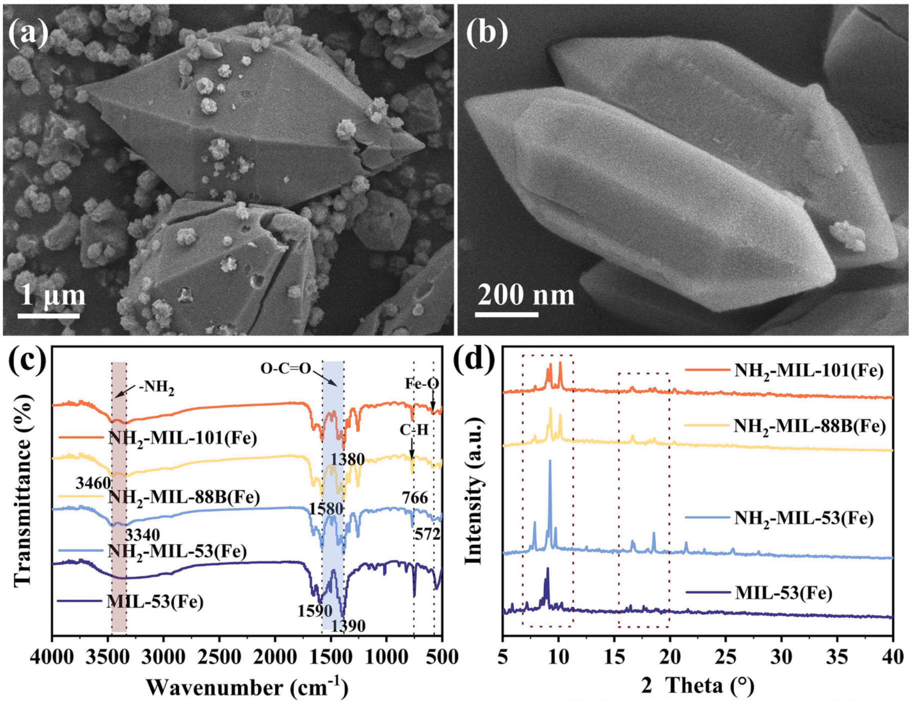

Fig. 1. SEM images of (a) MIL-53(Fe) and (b) NH_2-MIL-53(Fe). FT-IR spectra (c) and XRD patterns (d) of MIL-53(Fe), NH_2-MIL-53(Fe), NH_2-MIL-88(Fe) and NH_2-MIL-101(Fe).

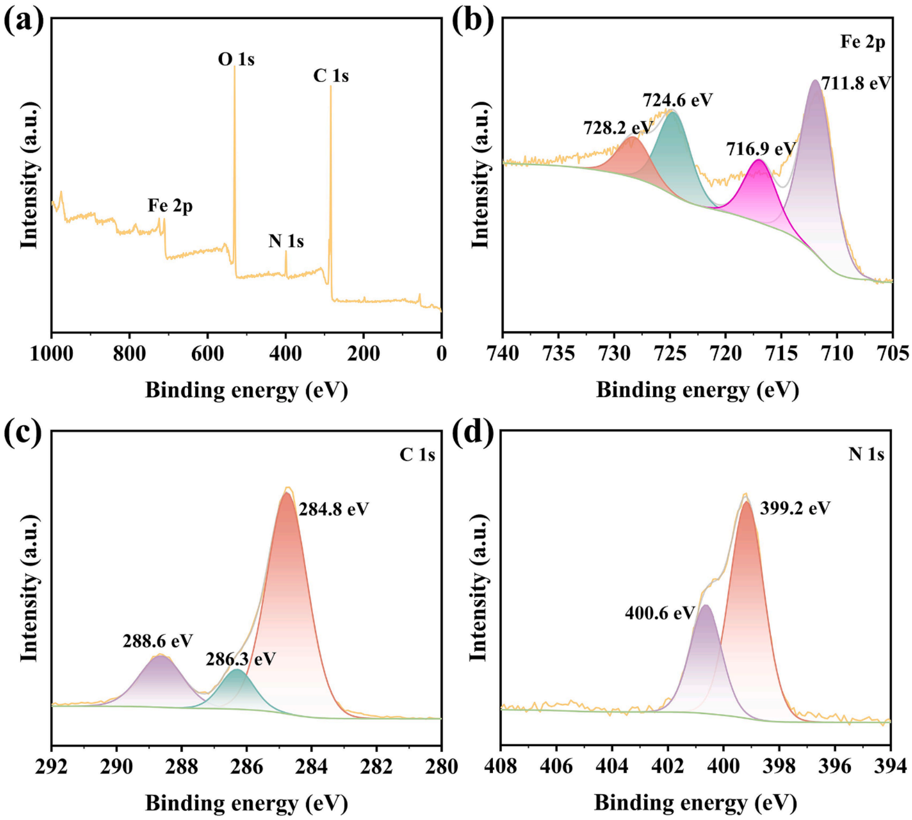

Fig. 2. The XPS spectra of NH_2-MIL-53(Fe): (a) survey, (b) Fe 2p, (c) C 1 s, (d) N 1 s.

To investigate potential reasons contributing to the differences in PFP among these amino-functionalized Fe-MOFs, several possible factors were considered. It is widely acknowledged that a suitable specific surface area and pore volume facilitates the access of more guest molecules to active sites. The N_2 adsorption–desorption isotherms were displayed in Fig. 4, all isotherms followed the typical type IV, suggesting the presence of mesoporous structures in amino-functionalized Fe-MOFs. The specific surface area and pore parameters were summarized

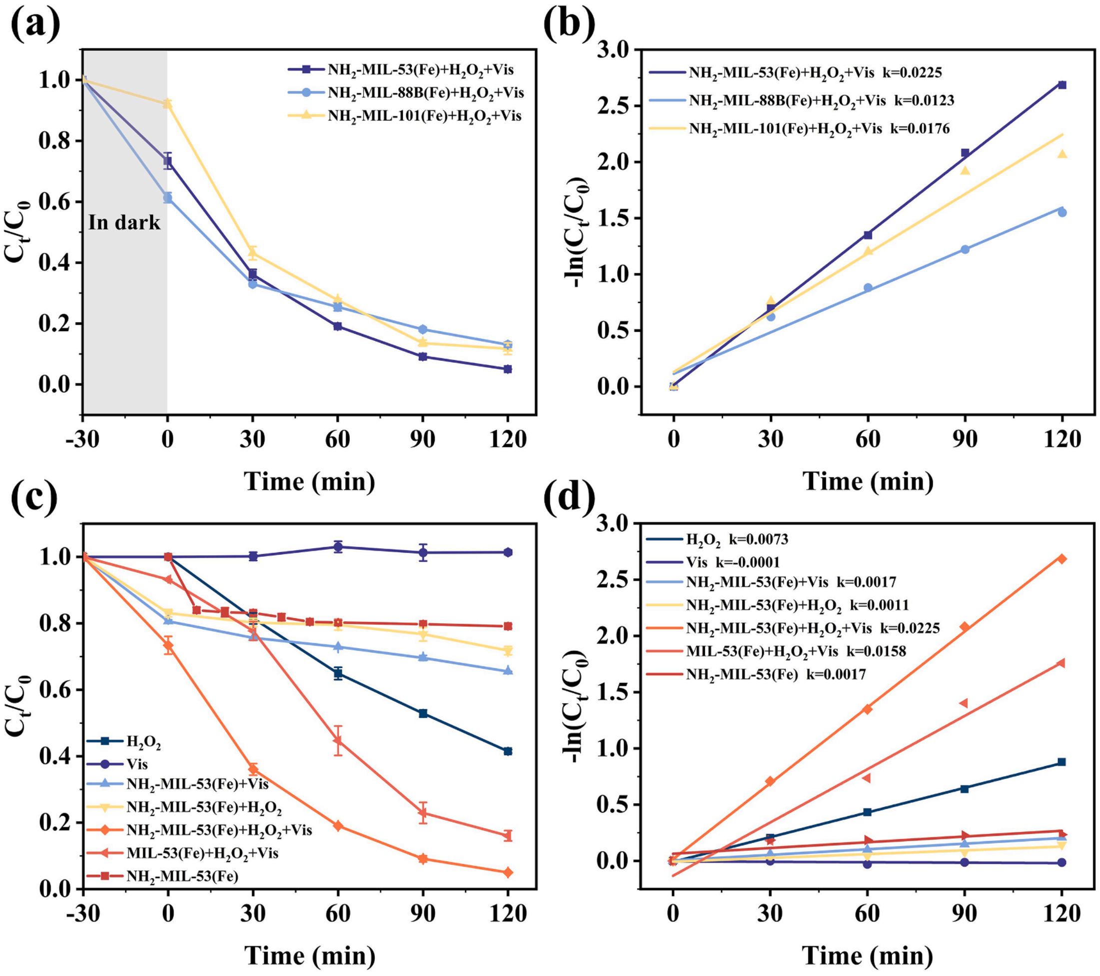

Fig. 3. (a) Degradation of RhB by photocatalysts, (b) the corresponding kinetics curves of photocatalysts. (c) Degradation of RhB in different systems, (d) the corresponding kinetics curves of different systems. Reaction conditions: RhB = 40 mg/L, pH = 3.0, Catalyst dosage = 0.08 g/L, H_2O_2 = 14 mM.

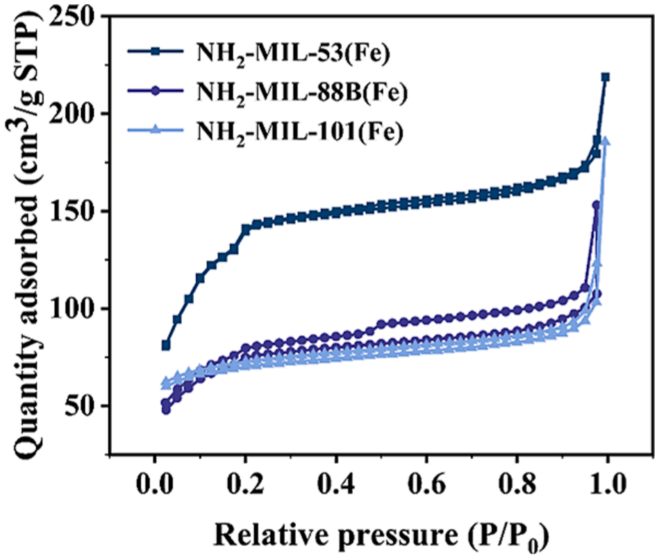

Fig. 4. N_2 adsorption–desorption isotherms of amino functionalization Fe-MOFs.

in Table 1. NH_2-MIL-53(Fe) had the largest specific surface area and pore volume, followed by NH_2-MIL-101(Fe) and NH_2-MIL-88B(Fe), in a sequence that corresponded well with their PFP.

Table 1
Summary BET data of the as-synthesized amino-functionalized Fe-MOFs.

Fe-MOFs	Surface area (m^2/g)	Pore volume (cm^3/g)	Pore size (nm)
NH_2-MIL-53(Fe)	348.87	0.26	3.10
NH_2-MIL-88B (Fe)	210.16	0.15	2.43
NH_2-MIL-101 (Fe)	329.18	0.15	1.91

Fig. S2 showed the photo-absorption properties of amino-functionalized Fe-MOFs. Absorbance intensity was in the sequence of NH_2-MIL-53(Fe) > NH_2-MIL-88B(Fe) > NH_2-MIL-101(Fe). It was consistent with the PFP.

The photoluminescence (PL) spectrum was shown in Fig. S3. PL was employed to validate the separation of carriers within amino-functionalized Fe-MOFs. In general, high PL intensities indicated rapid complexation of photogenerated electron-hole pairs. The PL intensity of NH_2-MIL-53(Fe) was the lowest.

As mentioned above, NH_2-MIL-53(Fe) exhibited enhanced responsiveness to visible-light and improved efficiency in charge separation, These characteristics promoted the transformation of Fe(III)/Fe(II) and improved the potential of Fenton reaction. Therefore, NH_2-MIL-53(Fe) could be one of the ideal materials for heterogeneous photo-Fenton reaction.

3.2.1. RhB degradation activity in different systems

Fig. 3**c** showed the degradation of RhB under different reaction systems. In the context of a system consisting of NH_2-MIL-53(Fe) and H_2O_2, a degradation rate of 28.2% was observed for RhB. Furthermore, NH_2-MIL-53(Fe) exhibited an adsorption capacity of approximately 20.9% for RhB, and when light and NH_2-MIL-53(Fe) were present, the degradation rate was 34.5%. Remarkably, the presence of NH_2-MIL-53 (Fe), H_2O_2 and light significantly increased the degradation rate of RhB to 95.0%. This finding suggested that the catalysts, H_2O_2 and visible light, exhibited a synergistic effect [53,54]. The photo-Fenton reaction was triggered by visible light irradiation, which facilitated the cyclic conversion of Fe(III)/Fe(II) through photogenerated electron-hole transfer [55]. To assess the reaction rate constant of RhB degradation, the experimental data underwent fitting using the pseudo-first-order equation (-ln $(C_t/C_0) = kt$) (Fig. 3**d**). The kinetic constant of the NH_2-MIL-53(Fe) + H_2O_2 + Vis system (0.0225 min^{-1}) exhibited higher values compared to those of MIL-53(Fe) system (0.0158 min^{-1}).

3.3. Influence factors on RhB degradation

To elucidate the most favorable reaction conditions for NH_2-MIL-53 (Fe) photo-Fenton, an investigation was conducted to assess the impact of various parameters. The effect of pH on RhB degradation process was investigated by adjusting initial pH of solution using 0.1 M H_2SO_4 or NaOH. As shown in Fig. 5**a** and Fig. 5**b**, the degradation rate of RhB exhibited its maximum value at pH = 3.0 within 120 min. When the initial pH was increased to 9.0 and 11.0, the degradation rate decreased to 74.2% and 51.0%, respectively. This might be attributed to the co-ordination of excess ·OH with the iron sites of NH_2-MIL-53(Fe), which are considered as Lewis bases [38]. Under alkaline conditions (pH = 9.0–11.0), the coordination and contact between H_2O_2 and the iron sites were impeded, resulting in a diminished generation of ·OH and causing a decline in the degradation rate of RhB. Additionally, it has been observed that iron precipitation can take place in environments with high alkalinity [56], leading to the deceleration of photo-Fenton reaction. Nevertheless, the degradation rate of RhB was above 82.0% within

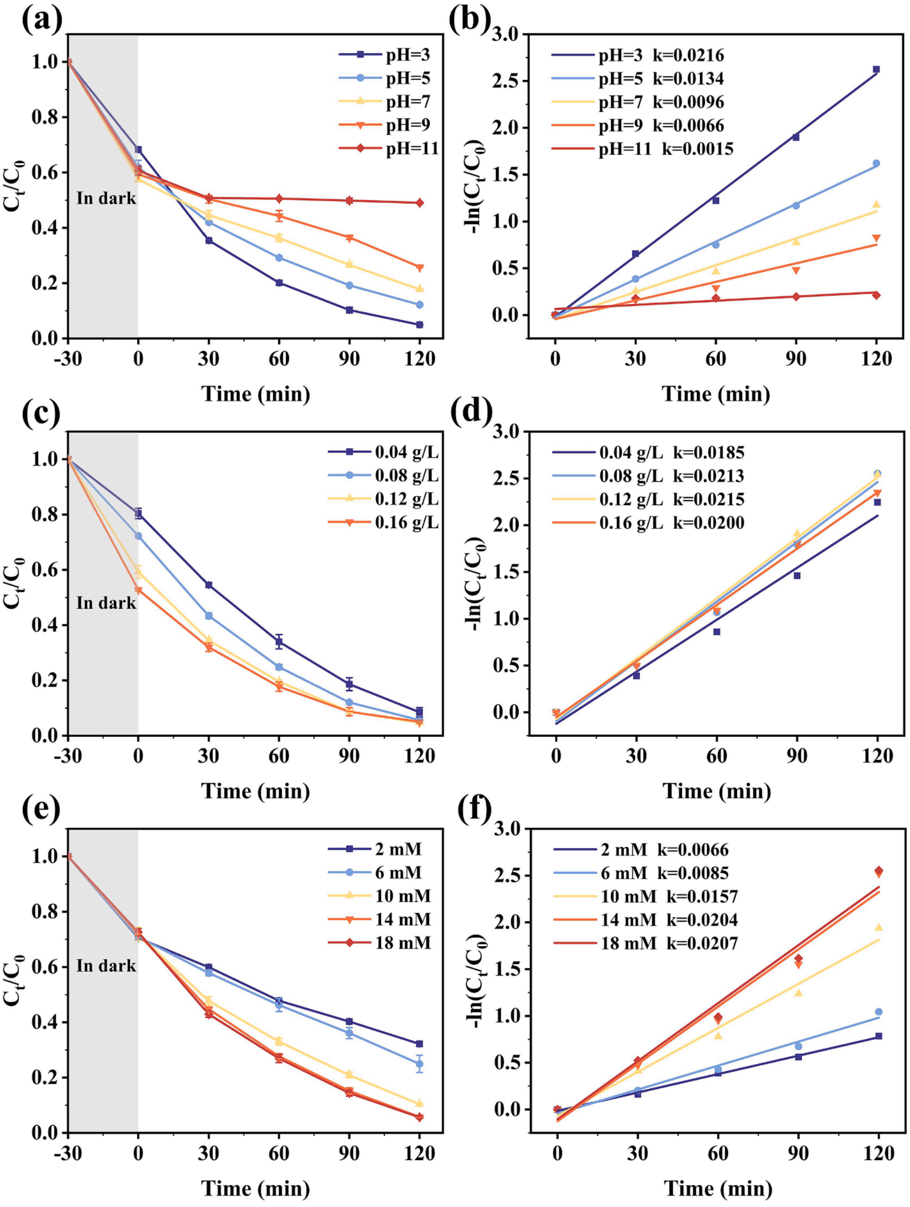

Fig. 5. (a) Effect of different initial pH. (b) the corresponding k values of pH. (c) Effect of different catalyst dosages. (d) the corresponding k values of catalyst dosages. (e) Effect of different H_2O_2 concentrations. (f) the corresponding k values of H_2O_2 concentrations. Final reaction conditions: RhB = 40 mg/L, pH = 3.0, catalyst dosage = 0.08 g/L, H_2O_2 = 14 mM. Note: only one factor was altered, and the other factors were fixed in the Fig. 5a, Fig. 5c and Fig. 5e.

the pH range of 3.0–7.0, highlighting the extensive pH adaptability of the reaction system.

The impact of catalyst dosage was investigated so as to clarify the optimal dosage. The results were displayed in Fig. 5**c** and Fig. 5**d**. The degradation rate of RhB gradually increased from 91.0% (0.0185 min^{-1}) to 95.0% (0.0213 min^{-1}) as the dosage of NH_2-MIL-53(Fe) was raised from 0.04 g/L to 0.08 g/L. This could be due to the increased catalyst providing more catalytic reaction sites [57]. However, the degradation rate constant decreased to 0.0200 min^{-1} when the catalyst dosage was further increased from 0.08 g/L to 0.16 g/L. This could be attributed to three aspects: (1) excess catalyst tended to aggregate, resulting in a decrease in active sites [58]; (2) excess catalyst increased the turbidity of the solution and affects the absorption of visible light, thus limiting the degradation activity; (3) the excess catalyst produced a large number of Fe(III) active sites, which reacted with H_2O_2 to generate a significant amount of Fe(II) and consumed ·OH (Fe(II) + ·OH → Fe(III) + OH^-), resulting in weakening of the oxidizing ability. Through these comparisons, it was determined that the optimal amount of catalyst to add for this photo-Fenton system was 0.08 g/L. In addition, compared with some literature reports [59,60], the usage of NH_2-MIL-53(Fe) was reduced while maintaining higher resource efficiency.

The impact of H_2O_2 concentration was investigated. The results were shown in Fig. 5**e** and Fig. 5**f**. With an increase in H_2O_2 concentration from 2 mM to 14 mM, the degradation rate of RhB exhibited a rapid enhancement (from 67.8% to 94.2%), and the related k value was increased from 0.0066 min^{-1} to 0.0204 min^{-1}, which was attributed to the generation of more ·OH. However, when further increased to 18 mM, the degradation rate remained almost unchanged. The phenomenon could be attributed to the reaction of excess H_2O_2 with ·OH, resulting in the formation of less reactive HO_2· (Eq. (1)-(2)) [61]. This reaction led to the consumption of ·OH and subsequently weaker catalytic activity [62]. Therefore, determining the optimal dosing concentration of H_2O_2 was very important to ensure maximum economic benefits in practical applications. The final concentration of H_2O_2 was selected as14 mM.

$$H_2O_2 + \cdot OH \rightarrow H_2O + HO_2(1)$$

$$HO_2\cdot + \cdot OH \rightarrow H_2O + O_2(2)$$

Coexisting inorganic anions in real aqueous environments may have an effect on the degradation of organic pollutants [63]. To further investigate the potential of the photo-Fenton system in practical applications, aqueous solution containing different inorganic anions (Cl^-、SO_4^{2-}、$H_2PO_4^-$) was dissolved in RhB solution to prepare simulated wastewater samples. The results were shown in Fig. 6**a**, Cl^- and SO_4^{2-} had no significant effect on RhB degradation. However, the addition of $H_2PO_4^-$ inhibited the degradation rate, amounting to approximately 15.4%. This might be attributed to the fact that $H_2PO_4^-$ can act as a scavenger for h^+ and ·OH [64]. And the addition of $H_2PO_4^-$ to the RhB solution resulted in a significant increase in pH from 3.0 to 8.0. This alteration in pH was found to be unfavorable for the generation of ·OH, consequently impeding the degradation process.

The performance of the NH_2-MIL-53(Fe) + H_2O_2 + Vis system was investigated for real water treatment by assessing the degradation of RhB in tap water and lake water. The lake water sample was obtained from Taihu River (Wuxi, China) and the tap water sample was acquired from the laboratory of Jiangnan University. According to the findings presented in Fig. 6**b**, when tap water and lake water were used, the degradation rate of RhB decreased by 15.3% and 5.8%, respectively. The decrease might be that these two water samples contained some organic carbon, which consumed certain free radicals for self-degradation [65]. Additionally, it was also possible that certain anions present in the water samples such as $H_2PO_4^-$ and HCO_3^- interfere with the degradation of RhB [64]. Overall, the degradation rate of RhB in actual water samples was still about 90.0% at most, indicating that the NH_2-MIL-53(Fe) + H_2O_2 + Vis system had great potential for practical wastewater treatment.

3.4. Reusability and stability

For practical applications, the stability and reusability of catalysts are crucial. The stability and reusability of NH_2-MIL-53(Fe) were evaluated by RhB degradation cycling experiments. The results were shown in Fig. 7**a**, indicating that the degradation rate remained notably high at 90.1% even after undergoing five cycles. Catalyst loss was unavoidable during the recovery process. This was only 4.9% lower than the first experiment. This indicated that the used catalyst had good stability and reusability. Meanwhile, the levels of dissolved metal ions in experiment were analyzed using the inductively coupled plasma mass spectrometry technique. It was observed that the concentration of leached iron ions exhibited an upward trend with increasing reaction time. However, the measured concentration (0.57 mg/L (Fig. 7**b**)) was significantly below the EU environmental emission standard (2.0 mg/L). In **Fig. S4**, after 8 h, the mineralization rate of RhB reached 78.0%. In Fig. 7**c** and Fig. 7**d**, the FT-IR and XRD spectra of before and after NH_2-MIL-53(Fe) were similar, which further demonstrated the used catalyst had excellent stability.

3.5. Degradation mechanism

3.5.1. Identification of active species

To gain insight into the reaction mechanism, the active species capture experiment was conducted. FFA, EDTA-2Na and TBA were used as the scavengers for the three reactive species of $^1O_2$, h^+ and ·OH, respectively [66]. As displayed in Fig. 8. The degradation rate exhibited different degrees of decreases after the introduction of scavengers. Among them, the degradation rate significantly decreased from 95.0% to 39.6% and 52.1% after the addition of FFA and TBA, respectively.

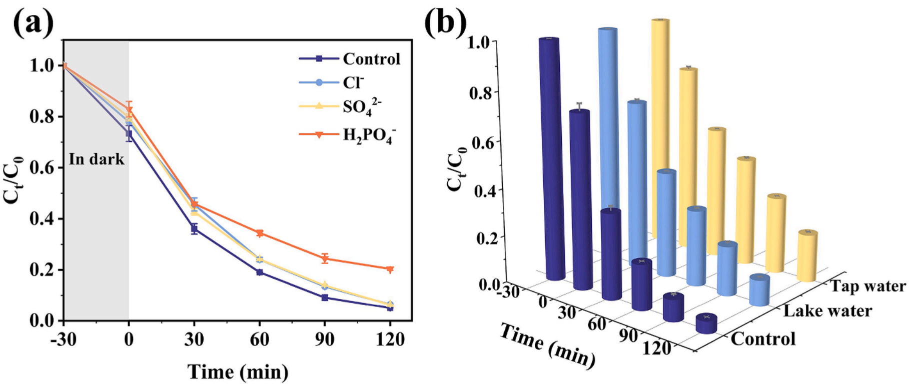

Fig. 6. (a) Effect of different inorganic anions. (b) Degradation of RhB in actual water samples. Reaction conditions: RhB = 40 mg/L, pH = 3.0, catalyst dosage = 0.08 g/L, H_2O_2 = 14 mM.

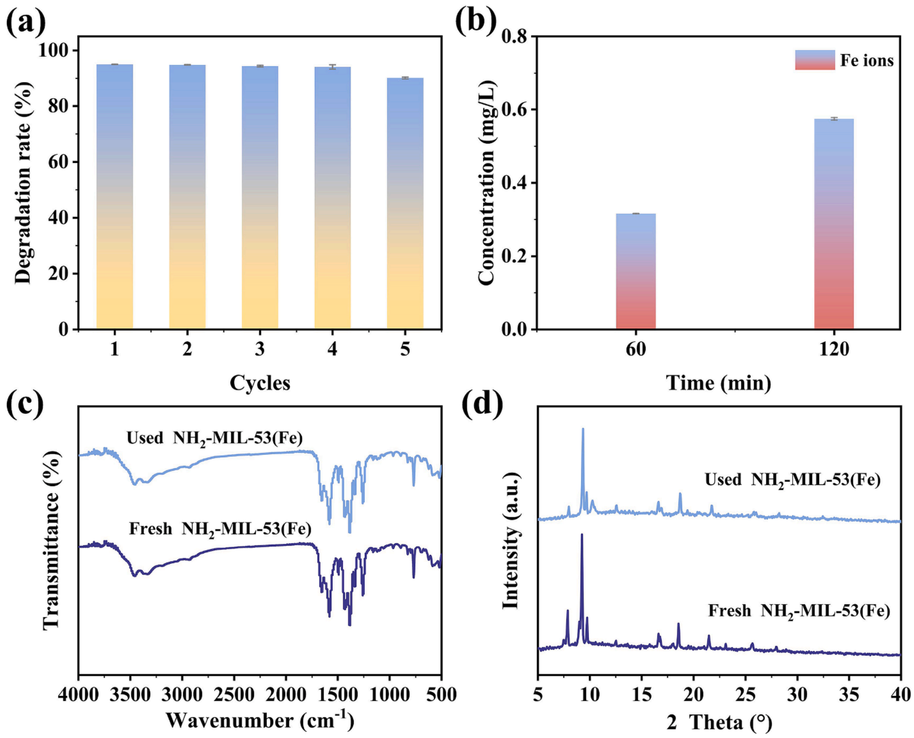

Fig. 7. (a) Cycle experiment of RhB degradation. (b) The dissolved metal ion concentration. (c) FT-IR spectrum and (d) XRD patterns of NH_2-MIL-53(Fe) before and after recycling test. Reaction conditions: RhB = 40 mg/L, pH = 3.0, catalyst dosage = 0.08 g/L, H_2O_2 = 14 mM.

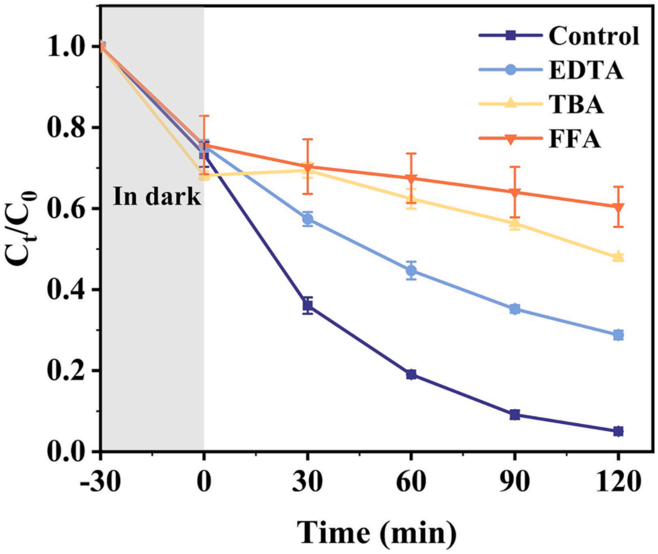

Fig. 8. Impacts of various scavengers on photo-Fenton degradation of RhB.

This indicated that $^1O_2$ and ·OH play a major role in photo-Fenton process.

3.5.2. *Degradation pathways and products of RhB*

The products were monitored to further assess the degradation pathway. According to the MS, ten products were identified. Ten products were named P1 ~ P10, as shown in **Table S3**. The degradation occurred through a series of reactions, including N-demethylation, deamination, dealkylation, decarboxylation, chromophore splitting, ring opening and mineralization [67].

The possible degradation pathways in this experiment were shown in Fig. 9. Pathway I: RhB (m/z = 443) was converted to P1 (m/z = 415) by demethylation reaction, then P1 was further demethylated to generate P2 (m/z = 387). Subsequently, P2 was converted to P3 (m/z = 318) by –NH bond breaking and demethylation reaction, followed by the deamination of P3 to generate P4 (m/z = 302). P4 further generated small molecule organic compounds P8 (m/z = 166) and P9 (m/z = 102) through decarboxylation and ring-opening reaction, and finally mineralized into CO_2 and H_2O. Pathway II: RhB (m/z = 443) was converted to P1 (m/z = 415) via demethylation reaction, and then the chromophore breakage of P1 produced P5 (m/z = 283) and P6 (m/z = 274). Subsequently, P5 and P6 produced P7 (m/z = 221) by ring opening and deamination reaction, then P7 through the ring-opening reaction further produced small molecule organic compounds, P8, P9 and P10 (m/z = 73), and finally mineralized into CO_2 and H_2O [65,68–70].

3.5.3. *RhB degradation mechanism in the NH_2-MIL-53(Fe) + H_2O_2 + Vis system*

Based on the above analysis, the possible mechanism of RhB degradation was proposed (Fig. 10). Firstly, NH_2-MIL-53(Fe) acted as a photocatalyst to generate (e^- and h^+) under visible light irradiation (Eq. (3)). A portion of h^+ migrated to the catalyst surface for direct degradation of RhB, while another fraction of h^+ formed ·OH by oxidizing H_2O (Eq. (4)) [71]. Photogenerated electrons (e^-) can directly react with H_2O_2 adsorbed on NH_2-MIL-53(Fe) to form ·OH (Eq. (5)). Secondly, in the photo-Fenton reaction, photogenerated electrons (e^-) can reduce Fe (III) to Fe(II) (Eq. (6)). Fe(III)/Fe(II) active center from NH_2-MIL-53(Fe) reacted with H_2O_2 to produce ·OH (Eq. (7)) and a slightly oxidizing ·OOH (Eq. (8)). The cyclic generation of ·OH made NH_2-MIL-53(Fe) catalyzed the photo-Fenton reaction with high reactivity. Additionally, ·OH could further generate $^1O_2$ (Eq. (9)), and RhB was degraded by ·OH, $^1O_2$ and h^+ to small molecule organic compounds that were ultimately degraded to CO_2 and H_2O. (Eq. (10)) [60,66].

$NH_2\text{-MIL-53(Fe)} + hv \rightarrow e^- + h^+$(3)

$h^+ + H_2O \rightarrow \cdot OH + H^+$(4)

$e^- + H_2O_2 \rightarrow \cdot OH + OH^-$(5)

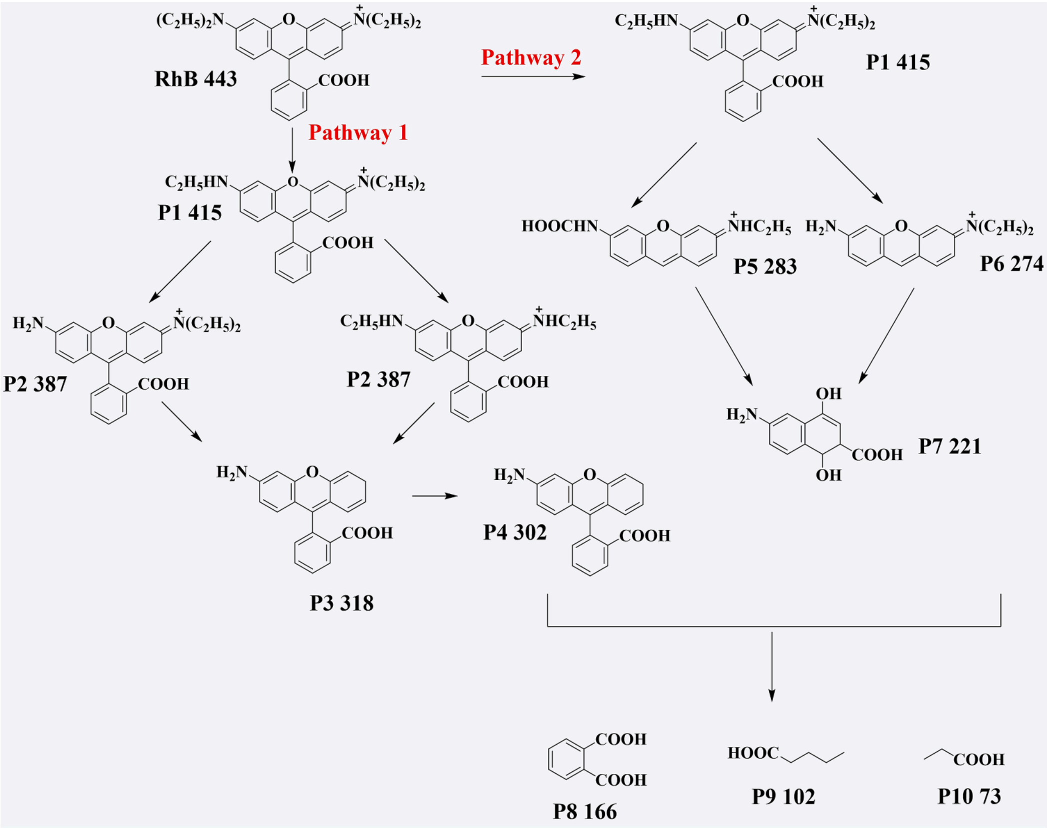

Fig. 9. The degradation pathway of RhB.

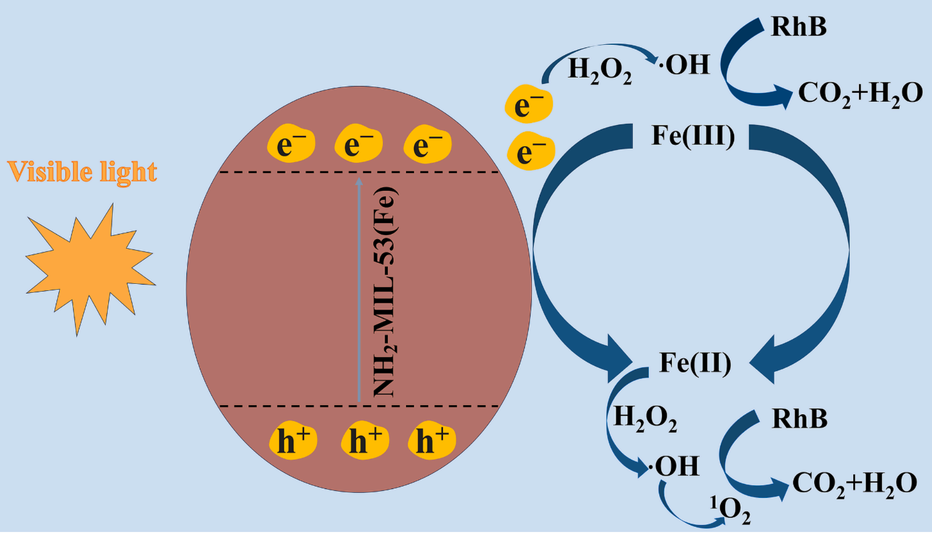

Fig. 10. The mechanism for degradation of RhB.

$Fe(III) + e^{-} \rightarrow Fe(II)$(6)

$Fe(II) + H_2O_2 \rightarrow Fe(III) + \cdot OH + OH^{-}$(7)

$Fe(III) + H_2O_2 \rightarrow Fe(II) + \cdot OOH + H^{+}$(8)

$4 \cdot OH \rightarrow {}^{1}O_2 + 2\ H_2O$(9)

$\cdot OH$ / ${}^{1}O_2$ / h^{+} + RhB → Small molecule organic → $CO_2 + H_2O$(10)

4. Conclusion

In summary, NH_2-MIL-53, NH_2-MIL-88B and NH_2-MIL-101 were synthesized and successfully used for photo-Fenton degradation RhB. NH_2-MIL-53(Fe) showed the best photo-Fenton catalytic performance, primarily due to its most suitable specific surface area and pore volume, as well as its superior light absorption properties. NH_2-MIL-53(Fe) could achieve efficient degradation of RhB (95.0%) in a wide pH (3.0–7.0) range and a short time (120 min). And after five consecutive cycling experiments, the degradation rate remained notably high at 90.1%. Free radical capture experiments showed that both ·OH and $^1O_2$ radicals were involved in the degradation of RhB. After 8 h, the mineralization rate of RhB reached 78.0%. More importantly, NH_2-MIL-53(Fe) showed low metal leaching, suggesting the environment friendliness. This study is expected to provide guidance for the selection of amino-functionalized photo-Fenton catalysts and demonstrate the great potential of NH_2-MIL-53(Fe) for practical applications. In future work, it will be necessary to continue to develop magnetic or hydrogel materials with stable catalytic performance in order to minimize the loss of catalyst during the recovery process.

CRediT authorship contribution statement

Lei-Qin Sun: Writing – original draft, Methodology, Investigation, Formal analysis, Conceptualization. **Xiao-Fang Shen:** Validation, Methodology, Investigation, Funding acquisition, Formal analysis. **Hong-Ming Zhang:** Methodology. **Yue-Hong Pang:** Writing – review & editing, Resources, Project administration, Funding acquisition, Conceptualization.

Declaration of competing interest

The authors declare that they have no known competing financial interests or personal relationships that could have appeared to influence the work reported in this paper.

Data availability

Data will be made available on request.

Acknowledgments

This work was supported by the National Natural Science Foundation of China (22276077, 21976070).

Appendix A. Supplementary data

Supplementary data to this article can be found online at https://doi.org/10.1016/j.jphotochem.2024.115544.

References

[1] M. Dulsat-Masvidal, C. Ciudad, O. Infante, R. Mateo, S. Lacorte, Water pollution threats in important bird and biodiversity areas from Spain, J. Hazard. Mater. 448 (2023) 130938, https://doi.org/10.1016/j.jhazmat.2023.130938.
[2] H.H. Wang, S.W. Yu, T. Gao, X.Y. Tan, X.G. Meng, S.J. Xiao, The efficient degradation of organic pollutants by Z-scheme MIL-88A@TiO_2 heterojunction photo-Fenton catalyst: The synergistic effect of photocatalysis and Fenton catalysis, J. Alloy. Compd. 960 (2023) 170688, https://doi.org/10.1016/j.jallcom.2023.170688.
[3] S.A. Hosseini, M. Vossoughi, N.M. Mahmoodi, M. Sadrzadeh, Clay-based electrospun nanofibrous membranes for colored wastewater treatment, Appl. Clay Sci. 168 (2019) 77–86, https://doi.org/10.1016/j.clay.2018.11.003.
[4] S.R. Aqdam, D.E. Otzen, N.M. Mahmoodi, D. Morshedi, Adsorption of azo dyes by a novel bio-nanocomposite based on whey protein nanofibrils and nano-clay: equilibrium isotherm and kinetic modeling, J. Colloid Interface Sci. 602 (2021) 490–503, https://doi.org/10.1016/j.jcis.2021.05.174.
[5] Z.D. Li, X.Y. Zhang, G.Z. Li, F.J. Han, D.Q. Hu, X.Y. Huang, H. Yuan, Y.Q. Tan, Hollow Co/CoO/Carbon nanofibers promoted PMS decomposition for the degradation of rhodamine B, J. Mater. Sci. Technol. 157 (2023) 120–129, https://doi.org/10.1016/j.jmst.2022.10.079.
[6] X. Peng, S. Xie, S.J. Xiong, R. Li, P. Wang, X.M. Zhang, Z.T. Liu, L.S. Hu, B. Gao, P. Kelly, P.K. Chu, Ultralow-voltage hydrogen production and simultaneous rhodamine B beneficiation in neutral wastewater, J. Energy Chem. 81 (2023) 574–582, https://doi.org/10.1016/j.jechem.2023.03.022.
[7] C. Lops, A. Ancona, K. Di Cesare, B. Dumontel, N. Garino, G. Canavese, S. Hérnandez, V. Cauda, Sonophotocatalytic degradation mechanisms of rhodamine B dye via radicals generation by micro- and nano-particles of ZnO, Appl. Catal. B 243 (2019) 629–640, https://doi.org/10.1016/j.apcatb.2018.10.078.
[8] O.P. Taran, A.N. Zagoruiko, S.A. Yashnik, A.B. Ayusheev, A.V. Pestunov, I. P. Prosvirin, R.V. Prihod'ko, V.V. Goncharuk, V.N. Parmon, Wet peroxide oxidation of phenol over carbon/zeolite catalysts. kinetics and diffusion study in batch and flow reactors, J. Environ. Chem. Eng. 6 (2018) 2551–2560, https://doi.org/10.1016/j.jece.2018.03.017.
[9] N.M. Mahmoodi, S. Keshavarzi, M. Ghezelbash, Synthesis of nanoparticle and modelling of its photocatalytic dye degradation ability from colored wastewater, J. Environ. Chem. Eng. 5 (2017) 3684–3689, https://doi.org/10.1016/j.jece.2017.07.010.
[10] A. Saravanan, P.S. Kumar, R.V. Hemavathy, S. Jeevanantham, M.J. Jawahar, J. P. Neshaanthini, R. Saravanan, A review on synthesis methods and recent applications of nanomaterial in wastewater treatment: challenges and future perspectives, Chemosphere 307 (2022) 135713, https://doi.org/10.1016/j.chemosphere.2022.135713.
[11] Z. Mokhtari-Shourijeh, S. Langari, L. Montazerghaem, N.M. Mahmoodi, Synthesis of porous aminated PAN/PVDF composite nanofibers by electrospinning: characterization and direct red 23 removal, J. Environ. Chem. Eng. 8 (2020) 103876, https://doi.org/10.1016/j.jece.2020.103876.
[12] Y. Wang, H.H. Li, W.N. Xia, L. Yu, Y. Yao, X.D. Zhang, H. Jiang, Synthesis of carbon microsphere-supported nano-zero-valent iron sulfide for enhanced removal of Cr (VI) and p-nitrophenol complex contamination in peroxymonosulfate system, J. Mol. Liq. 390 (2023) 123089, https://doi.org/10.1016/j.molliq.2023.123089.
[13] D. Xu, H.L. Ma, Degradation of rhodamine B in water by ultrasound-assisted TiO_2 photocatalysis, J. Clean. Prod. 313 (2021) 127758, https://doi.org/10.1016/j.jclepro.2021.127758.
[14] Z.B. Wang, H.B. Wang, P. Wang, X.W. Liu, X.F. Lei, R. Guo, J.H. You, H.Z. Zhang, Application of MOFs driven by various energy sources for degradation the organic pollutants in water: a review, Coord. Chem. Rev. 499 (2024) 215506, https://doi.org/10.1016/j.ccr.2023.215506.
[15] J.F. Bao, S.S. Guo, D.D. Fan, J.L. Cheng, Y. Zhang, X. Pang, Sonoactivated nanomaterials: a potent armament for wastewater treatment, Ultrason. Sonochem. 99 (2023) 106569, https://doi.org/10.1016/j.ultsonch.2023.106569.
[16] Y.W. Kang, K.Y. Hwang, Effects of reaction conditions on the oxidation efficiency in the Fenton process, Water Res. 34 (2000) 2786–2790, https://doi.org/10.1016/S0043-1354(99)00388-7.
[17] H. Weng, Y. Yang, C. Zhang, M. Cheng, W.J. Wang, B. Song, H.Z. Luo, D.Y. Qin, C. Huang, F.Z. Qin, K.T. Li, Insight into FeOOH-mediated advanced oxidation processes for the treatment of organic polluted wastewater, Chem. Eng. J. 453 (2023) 139812, https://doi.org/10.1016/j.cej.2022.139812.
[18] Y. Wang, N.P. Lin, J. Xu, H. Jiang, R.Z. Chen, X.D. Zhang, N. Liu, Construction of microwave/PMS combined dual responsive perovskite-MXene system for antibiotic degradation: synergistic effects of thermal and non-thermal, Appl. Surf. Sci. 639 (2023) 158263, https://doi.org/10.1016/j.apsusc.2023.158263.
[19] Y. Wang, H.H. Li, J. Xu, J.Y. Yu, J.F. Wang, H. Jiang, C.Y. Li, X.D. Zhang, N. Liu, High-performance carbon@ metal oxide nanocomposites derived metal-organic framework-perovskite hybrid boosted microwave-induced catalytic degradation of norfloxacin: performance, degradation pathway and mechanism, Sep. Purif. Technol. 330 (2024) 125399, https://doi.org/10.1016/j.seppur.2023.125399.
[20] P.V. Gayathri, S. Yesodharan, E.P. Yesodharan, Microwave/Persulphate assisted ZnO mediated photocatalysis (MW/PS/UV/ZNO) as an efficient advanced oxidation process for the removal of RhB dye pollutant from water, J. Environ. Chem. Eng. 7 (2019) 103122, https://doi.org/10.1016/j.jece.2019.103122.
[21] M.H. Zhang, H. Dong, L. Zhao, D.X. Wang, D. Meng, A review on Fenton process for organic wastewater treatment based on optimization perspective, Sci. Total Environ. 670 (2019) 110–121, https://doi.org/10.1016/j.scitotenv.2019.03.180.
[22] N. Thomas, D.D. Dionysiou, S.C. Pillai, Heterogeneous Fenton catalysts: a review of recent advances, J. Hazard. Mater. 404 (2021) 124082, https://doi.org/10.1016/j.jhazmat.2020.124082.
[23] Q.S. Wu, M.S. Siddique, H.J. Wang, L.Q. Cui, H. Wang, M. Pan, J.L. Yan, Visible-light-driven iron-based heterogeneous photo-Fenton catalysts for wastewater decontamination: a review of recent advances, Chemosphere 313 (2023) 137509, https://doi.org/10.1016/j.chemosphere.2022.137509.
[24] H.I. Hamoud, P. Damacet, D. Fan, N. Assaad, O.I. Lebedev, A. Krystianiak, A. Gouda, O. Heintz, M. Daturi, G. Maurin, M. Hmadeh, M. El-Roz, Selective photocatalytic dehydrogenation of formic acid by an in situ-restructured copper-postmetalated metal-organic framework under visible light, J. Am. Chem. Soc. 144 (2022) 16433–16446, https://doi.org/10.1021/jacs.2c04905.
[25] X. Zhang, B. Gao, R. Rao, F. Bi, C. Li, K. Yue, Y. Wang, J. Xu, X. Feng, Y. Yang, Defects materials of institut Lavoisier-125(Ti) materials enhanced photocatalytic activity for toluene and chlorobenzene mixtures degradation: mechanism study, J. Colloid Interface Sci. 660 (2024) 423–439, https://doi.org/10.1016/j.jcis.2024.01.012.
[26] C. Wu, V.K.M. Au, Efficient removal of piroxicam and ketoprofen by acid-modulated iron(III) metal-organic frameworks, J. Ind. Eng. Chem. 129 (2024) 544–554, https://doi.org/10.1016/j.jiec.2023.09.013.
[27] J. Li, Q.K. Lv, L.L. Bi, F. Fang, J.F. Hou, G.L. Di, J. Wei, X.W. Wu, X.D. Li, Metal-organic frameworks as superior adsorbents for pesticide removal from water: the cutting-edge in characterization, tailoring, and application potentials, Coord. Chem. Rev. 493 (2023) 215303, https://doi.org/10.1016/j.ccr.2023.215303.
[28] N. Prasetya, I.G. Wenten, M. Franzreb, C. Wöll, Metal-organic frameworks for the adsorptive removal of pharmaceutically active compounds (PhACs): comparison to activated carbon, Coord. Chem. Rev. 475 (2023) 214877, https://doi.org/10.1016/j.ccr.2022.214877.
[29] S. Navalón, A. Dhakshinamoorthy, M. Alvaro, B. Ferrer, H. García, Metal-organic frameworks as photocatalysts for solar-driven overall water splitting, Chem. Rev. 123 (2023) 445–490, https://doi.org/10.1021/acs.chemrev.2c00460.
[30] C. Liu, H.R.Q. Liu, J.C. Yu, L. Wu, Z.H. Li, Strategies to engineer metal-organic frameworks for efficient photocatalysis, Chin. J. Catal. 55 (2023) 1–19, https://doi.org/10.1016/S1872-2067(23)64556-5.

[31] K.G.M. Laurier, F. Vermoortele, R. Ameloot, D.E. De Vos, J. Hofkens, M.B. J. Roeffaers, Iron(III)-based metal-organic frameworks as visible light photocatalysts, J. Am. Chem. Soc. 135 (2013) 14488–14491, https://doi.org/10.1021/ja405086e.

[32] D.K. Wang, Z.H. Li, Iron-based metal-organic frameworks (MOFs) for visible-light-induced photocatalysis, Res. Chem. Intermed. 43 (2017) 5169–5186, https://doi.org/10.1007/s11164-017-3042-0.

[33] Y. Gong, B. Yang, H. Zhang, X. Zhao, A g-C_3N_4/MIL-101(Fe) heterostructure composite for highly efficient BPA degradation with persulfate under visible light irradiation, J. Mater. Chem. A 6 (2018) 23703–23711, https://doi.org/10.1039/C8TA07915C.

[34] Y. Horiuchi, T. Toyao, K. Miyahara, L. Zakary, D.D. Van, Y. Kamata, T.H. Kim, S. W. Lee, M. Matsuoka, Visible-light-driven photocatalytic water oxidation catalysed by iron-based metal-organic frameworks, ChemComm 52 (2016) 5190–5193, https://doi.org/10.1039/C6CC00730A.

[35] S.W. Lv, J.M. Liu, N. Zhao, C.Y. Li, Z.H. Wang, S. Wang, Benzothiadiazole functionalized Co-doped MIL-53-NH_2 with electron deficient units for enhanced photocatalytic degradation of bisphenol A and ofloxacin under visible light, J. Hazard. Mater. 387 (2020) 122011, https://doi.org/10.1016/j.jhazmat.2019.122011.

[36] C. Gao, Y. Su, X. Quan, V.K. Sharma, S. Chen, H.T. Yu, Y.B. Zhang, J.F. Niu, Electronic modulation of iron-bearing heterogeneous catalysts to accelerate Fe (III)/Fe(II) redox cycle for highly efficient Fenton-like catalysis, Appl. Catal. B 276 (2020) 119016, https://doi.org/10.1016/j.apcatb.2020.119016.

[37] X.S. Wang, G.J. Chen, H.J. Wang, Y. Wu, X.Q. Wei, J. Wen, L.Y. Hu, W.L. Gu, C. Z. Zhu, Imide modification coupling with NH_2-MIL-53(Fe) boosts the photocatalytic performance of graphitic carbon nitride for efficient water remediation, J. Catal. 399 (2021) 192–200, https://doi.org/10.1016/j.jcat.2021.05.007.

[38] H. Liu, H. Yin, X.L. Yu, M.H. Zhu, Z. Dang, Amino-functionalized MIL-88B as heterogeneous photo-Fenton catalysts for enhancing tris-(2-chloroisopropyl) phosphate (TCPP) degradation: dual excitation pathways accelerate the conversion of $\equiv Fe^{III}$ to $\equiv Fe^{II}$ under visible light irradiation, J. Hazard. Mater. 425 (2022) 127782, https://doi.org/10.1016/j.jhazmat.2021.127782.

[39] L.Y. Shao, Z.X. Yu, X.H. Li, X.Y. Li, H.J. Zeng, X.F. Feng, Carbon nanodots anchored onto the metal-organic framework NH_2-MIL-88B (Fe) as a novel visible light-driven photocatalyst: photocatalytic performance and mechanism investigation, Appl. Surf. Sci. 505 (2020) 144616, https://doi.org/10.1016/j.apsusc.2019.144616.

[40] Y.X. Wang, Z. Zhong, Y. Muhammad, H. He, Z.X. Zhao, S.X. Nie, Z.X. Zhao, Defect engineering of NH_2-MIL-88B(Fe) using different monodentate ligands for enhancement of photo-Fenton catalytic performance of acetamiprid degradation, Chem. Eng. J. 398 (2020) 125684, https://doi.org/10.1016/j.cej.2020.125684.

[41] M. Liu, Q.L. Huang, L. Li, G.P. Zhu, X.J. Yang, S.X. Wang, Cerium-doped MIL-101-NH_2(Fe) as superior adsorbent for simultaneous capture of phosphate and As(V) from yangzonghai coastal spring water, J. Hazard. Mater. 423 (2022) 126981, https://doi.org/10.1016/j.jhazmat.2021.126981.

[42] N. Liu, J.L. Wang, J.X. Wu, Z.M. Li, W.Y. Huang, Y.J. Zheng, J.Q. Lei, X.D. Zhang, L. Tang, Magnetic Fe_3O_4@MIL-53(Fe) nanocomposites derived from MIL-53(Fe) for the photocatalytic degradation of ibuprofen under visible light irradiation, Mater. Res. Bull. 132 (2020) 111000, https://doi.org/10.1016/j.materresbull.2020.111000.

[43] L. Zhu, Y. Chen, X. Liu, Y.Y. Si, Y.X. Tang, X. Wang, MoS_2-modified MIL-53(Fe) for synergistic adsorption-photocatalytic degradation of tetracycline, Environ. Sci. Pollut. Res. 30 (2023) 23086–23095, https://doi.org/10.1007/s11356-022-23859-z.

[44] Y.C. Xie, J.N. Wan, Z.C. Yan, Y. Wang, T. Xiao, J. Hou, Targeted degradation of sulfamethoxazole in wastewater by molecularly imprinted MOFs in advanced oxidation processes: degradation pathways and mechanism, Chem. Eng. J. 429 (2022) 132237, https://doi.org/10.1016/j.cej.2021.132237.

[45] B.F. Rad, H. Mahdavi, M.F. Rad, M. Baghdadi, Using design-expert to optimize the properties of a polyethersulfone ultrafiltration membrane through the incorporation of NH_2-MIL-53(Fe) and PVP for maximum Cr(VI) removal and flux, J. Polym. Environ. 30 (2022) 3875–3889, https://doi.org/10.1007/s10924-022-02477-3.

[46] N. Li, Y.Y. Yu, Y.Y. Zhou, K.X. Xu, Y.S. Zhou, L.J. Zhang, Y.X. Zhong, Construction of a logic gate computation and visual test paper for methyl paraoxon assay based on a fluorescent europium-organic framework, J. Mater. Chem. C (2024), https://doi.org/10.1039/D3TC04128J.

[47] A. Bagheri, H. Hoseinzadeh, B. Hayati, N.M. Mahmoodi, E. Mehraeen, Post-synthetic functionalization of the metal-organic framework: clean synthesis, pollutant removal, and antibacterial activity, J. Environ. Chem. Eng. 9 (2021) 104590, https://doi.org/10.1016/j.jece.2020.104590.

[48] N.M. Mahmoodi, M.H. Saffar-Dastgerdi, B. Hayati, Environmentally friendly novel covalently immobilized enzyme bionanocomposite: from synthesis to the destruction of pollutant, Compos. B Eng. 184 (2020) 107666, https://doi.org/10.1016/j.compositesb.2019.107666.

[49] X.Y. Wang, W. Zhang, X. Zhang, L. Ran, Q.L. Zhao, B.Z. Zou, L.C. Zhou, Z.F. Ye, A novel design of self-assembled metal-organic frameworks MIL-53(Fe) modified resin as a catalyst for catalytic degradation of tetracycline, J. Clean. Prod. 348 (2022) 131385, https://doi.org/10.1016/j.jclepro.2022.131385.

[50] T.V. Tran, V.H. Nguyen, L.X. Nong, H.T.T. Nguyen, D.T.C. Nguyen, T.T. Nguyen, H. T.T. Nguyen, T.D. Nguyen, Hexagonal Fe-based MIL-88B nanocrystals with NH_2 functional groups accelerating oxytetracycline capture via hydrogen bonding, Surf. Interfaces 20 (2020) 100605, https://doi.org/10.1016/j.surfin.2020.100605.

[51] N. Mahendran, K. Praveen, $BiPO_4$/Fe-metal organic framework composite: a promising photocatalyst toward the abatement of tetracycline hydrochloride, indigo carmine and reduction of 4-nitrophenol, J. Ind. Eng. Chem. 100 (2021) 220–232, https://doi.org/10.1016/j.jiec.2021.05.020.

[52] D.D. Wang, H.J. Li, Q. Han, W. Jiang, C.B. Liu, G.B. Che, Optimized design of $BiVO_4$/NH_2-MIL-53(Fe) heterostructure for enhanced photocatalytic degradation of methylene blue and ciprofloxacin under visible light, J. Phys. Chem. Solid 154 (2021) 110027, https://doi.org/10.1016/j.jpcs.2021.110027.

[53] Q.S. Wu, H.P. Yang, L. Kang, Z. Gao, F.F. Ren, Fe-based metal-organic frameworks as Fenton-like catalysts for highly efficient degradation of tetracycline hydrochloride over a wide pH range: acceleration of Fe(II)/Fe(III) cycle under visible light irradiation, Appl. Catal. B 263 (2020) 118282, https://doi.org/10.1016/j.apcatb.2019.118282.

[54] M. Cheng, C. Lai, Y. Liu, G.M. Zeng, D.L. Huang, C. Zhang, L. Qin, L. Hu, C.Y. Zhou, W.P. Xiong, Metal-organic frameworks for highly efficient heterogeneous Fenton-like catalysis, Coord. Chem. Rev. 368 (2018) 80–92, https://doi.org/10.1016/j.ccr.2018.04.012.

[55] Z. Mohammadifard, R. Saboori, N.S. Mirbagheri, S. Sabbaghi, Heterogeneous photo-Fenton degradation of formaldehyde using MIL-100(Fe) under visible light irradiation, Environ. Pollut. 251 (2019) 783–791, https://doi.org/10.1016/j.envpol.2019.04.143.

[56] X. Qin, K.X. Wang, P.K. Cao, Y. Su, S. Chen, H.T. Yu, X. Quan, Highly efficient electro-Fenton process on hollow porous carbon spheres enabled by enhanced H_2O_2 production and Fe^{2+} regeneration, J. Hazard. Mater. 446 (2023) 130664, https://doi.org/10.1016/j.jhazmat.2022.130664.

[57] Q.S. Wu, M.S. Siddique, Y.L. Guo, M. Wu, Y.K. Yang, H.P. Yang, Low-crystalline bimetallic metal-organic frameworks as an excellent platform for photo-Fenton degradation of organic contaminants: Intensified synergism between hetero-metal nodes, Appl. Catal. B 286 (2021 119950), doi:10.1016/j.apcatb.2021.119950.

[58] N.M. Mahmoodi, B. Karimi, M. Mazarji, H. Moghtaderi, Cadmium selenide quantum dot-zinc oxide composite: synthesis, characterization, dye removal ability with UV irradiation, and antibacterial activity as a safe and high-performance photocatalyst, J. Photochem. Photobiol. B Biol. 188 (2018) 19–27, https://doi.org/10.1016/j.jphotobiol.2018.08.023.

[59] Y.J. Yan, R.H. Wang, M. Maimaitituersun, H.J. Sun, X.F. Liu, Built-in electric field enhanced $BiFeO_3$ photo-Fenton degradation rhodamine B solution, J. Mater. Sci. 57 (2022) 6900–6913, https://doi.org/10.1007/s10853-022-06916-3.

[60] J.Y. Zhang, M.W. Yan, G.C. Sun, X. Li, B.L. Hao, K.Q. Liu, Mg-Fe-Al-O spinel: preparation and application as a heterogeneous photo-Fenton catalyst for degrading Rhodamine B, Chemosphere 304 (2022) 135318, https://doi.org/10.1016/j.chemosphere.2022.135318.

[61] B. Rabeie, N.M. Mahmoodi, Heterogeneous MIL-88A on MIL-88B hybrid: a promising eco-friendly hybrid from green synthesis to dual application (adsorption and photocatalysis) in tetracycline and dyes removal, J. Colloid Interface Sci. 654 (2024) 495–522, https://doi.org/10.1016/j.jcis.2023.10.060.

[62] Q. Wang, P. Wang, P. Xu, Y. Li, J.J. Duan, G.S. Zhang, L.M. Hu, X.J. Wang, W. Zhang, Visible-light-driven photo-Fenton reactions using $Zn_{1-1.5x}Fe_xS$/g-C_3N_4 photocatalyst: degradation kinetics and mechanisms analysis, Appl. Catal. B 266 (2020) 118653, https://doi.org/10.1016/j.apcatb.2020.118653.

[63] J. Hang, X.H. Yi, C.C. Wang, H.F. Fu, P. Wang, Y.J. Zhao, N.B. Saleh, Heterogeneous photo-Fenton degradation toward sulfonamide matrix over magnetic Fe_3S_4 derived from MIL-100(Fe), J. Hazard. Mater. 424 (2022) 127415, https://doi.org/10.1016/j.jhazmat.2021.127415.

[64] X.F. Li, X.L. Shen, Y.L. Qiu, Z.L. Zhu, H. Zhang, D.Q. Yin, Fe_3O_4 quantum dots mediated P-g-C_3N_4/BiOI as an efficient and recyclable Z-scheme photo-Fenton catalyst for tetracycline degradation and bacterial inactivation, J. Hazard. Mater. 456 (2023) 131677, https://doi.org/10.1016/j.jhazmat.2023.131677.

[65] H. Cheng, X.Y. Li, C. Huang, J. Zhu, P. Wang, H. Cao, C.L. Feng, D.X. Ling, H. Liu, M. Cheng, Accelerated Fe(III)/Fe(II) cycle for rapid elimination of Rhodamine B by a novel Mo_2C co-catalytic Fe^{2+}/H_2O_2 system, J. Clean. Prod. 393 (2023) 136354, https://doi.org/10.1016/j.jclepro.2023.136354.

[66] Z.M. Fang, Y.B. Liu, J.J. Qi, Z.F. Xu, T.Y. Qi, L.D. Wang, Establishing a high-speed electron transfer channel via CuS/MIL-Fe heterojunction catalyst for photo-Fenton degradation of acetaminophen, Appl. Catal. B 320 (2023) 121979, https://doi.org/10.1016/j.apcatb.2022.121979.

[67] V. Thirupugazhmani, S. Shameena, K. Thirumalai, A. Ravi, P.A. Vivekanand, P. Kamaraj, N. Arumugam, A.I. Almansour, R.S. Kumar, S.I. Alaqeel, K. Perumal, Ultrasonic assisted synthesis of RGO supported $HoVO_4$-ZnO nanocomposites, their enhanced photocatalytic activities and rhodamine B degradation, Environ. Res. 214 (2022) 113743, https://doi.org/10.1016/j.envres.2022.113743.

[68] T. Rasheed, M. Bilal, H.M.N. Iqbal, S.Z.H. Shah, H.B. Hu, X.H. Zhang, Y.F. Zhou, TiO_2/UV-assisted rhodamine B degradation: putative pathway and identification of intermediates by UPLC/MS, Environ. Technol. 39 (2018) 1533–1543, https://doi.org/10.1080/09593330.2017.1332109.

[69] N. Guo, H.Y. Liu, Y. Fu, J.S. Hu, Preparation of Fe_2O_3 nanoparticles doped with In_2O_3 and photocatalytic degradation property for rhodamine B, Optik 201 (2020) 163537, https://doi.org/10.1016/j.ijleo.2019.163537.

[70] Y.C. Ren, P. Lu, G.F. Qu, P. Ning, N.Q. Ren, J. Wang, F.H. Wu, X.P. Chen, Z. L. Wang, T. Zhang, M.H. Cheng, X.M. Chu, Study on the mechanism of rapid degradation of Rhodamine B with Fe/Cu@antimony tailing nano catalytic particle electrode in a three dimensional electrochemical reactor, Water Res. 244 (2023) 120487, https://doi.org/10.1016/j.watres.2023.120487.

[71] J.Y. Zheng, C. Liu, Z.W. Wang, Y.Z. Shi, Y.D. Hou, J.H. Bi, L. Wu, Improving photocatalytic degradation of enrofloxacin over TiO_2 nanosheets with Ti^{3+} sites by coordination activation, Appl. Catal. A-Gen 660 (2023) 119217, https://doi.org/10.1016/j.apcata.2023.119217.